JOURNAL OF Materials CHEMISTRY

An experimental and theoretical investigation into the reflection spectra of SmC* and SmC_A* phases

Nicholas W. Roberts,[a] Helen F. Gleeson,*[a] Nicholas Bowring,[b] Alexander Seed,[c] L. N. Nassif,[c] M. R. Herbert,[c] John W. Goodby[d] and Mike Hird[d]

[a]*Department of Physics and Astronomy, The University of Manchester, Manchester, UK M13 9PL. E-mail: helen.gleeson@man.ac.uk*
[b]*Department of Computer Science, Leeds Metropolitan University, City Campus, Calverley Street, Leeds, UK LS1 3HE*
[c]*Department of Chemistry, Kent State University, OH 44242-0001, USA*
[d]*Department of Chemistry, The University of Hull, Hull, UK HU6 7RJ*

Received 2nd September 2002, Accepted 11th December 2002
First published as an Advance Article on the web 9th January 2003

Analysis of the reflection spectra of chiral smectic liquid crystal phases is used to provide detailed information on physical parameters, including refractive indices, helicoidal pitch and tilt angle. Numerical models of the antiferroelectric and ferroelectric phases are constructed, based on a 4 × 4 matrix technique, and a downhill simplex algorithm is employed to fit the model to reflection spectra measured from free-standing films of the materials of interest. The temperature dependence of the refractive indices, dispersion, tilt angle and pitch are reported for three different liquid crystalline materials. The accuracy of the fitting method is around 1%, better than the experimental error, and this is confirmed by comparison of the parameters determined by the fitting program with those measured by independent methods.

Introduction

For many years, optical investigations of liquid crystals have been central to the analysis of their structure and physical properties. One of the earliest examples of such an approach was the analysis of the selective reflection of light from a cholesteric liquid crystal by de Vries,[1] who deduced an optical model of the system and used it to relate the width and position of the reflection band to the helicoidal pitch and refractive indices of the system. Detailed analysis of the reflection band of chiral liquid crystals has proven to be an excellent technique for providing a fundamental understanding of helicoidal anisotropic structures[2–4] and experimental information relating to the physical properties.[5,6] In cholesteric liquid crystals, both aspects have been extensively explored, but there are few reports of the same approach being used to obtain quantitative information about the chiral smectic C* (SmC*) phases.[7–10]

Several SmC* liquid crystal subphases exist, each distinguished by specific interlayer molecular ordering.[11] The ferroelectric phase is helicoidal, with the average molecular direction (the director) tilted with respect to the layer normal by an angle known as the tilt angle. The direction of tilt is approximately the same from one smectic layer to the next, modified only by the macroscopic helix, which is typically hundreds of layers long. The antiferroelectric liquid crystal phase (SmC^*_A) is also helicoidal and differs from the SmC* phase in that the director in alternate layers tilts in (approximately) opposite directions. Both the tilt angle and helicoidal pitch in the SmC* and SmC^*_A phases are temperature dependent.

Previous optical studies[7–10] of chiral smectic phases concentrated on measuring the wavelength dependence of the centre of the reflection band as a function of temperature. Analysis of the reflection spectra to obtain other physical properties of these systems has largely been neglected. The aim of this paper is to report the physical properties of three different smectic liquid crystals, deduced from their selective reflection spectra using a powerful numerical fitting technique. The selective reflection spectra were measured at normal incidence as functions of the temperature and polarisation state of the incident light. The data obtained were analysed in the context of a 4 × 4 numerical matrix method.[2] Several other measurements, including ellipsometry,[12] optical rotatory power,[13] optical mode guiding[14–16] and resonant X-ray scattering,[17,18] have all recently been used to deduce the physical properties of liquid crystals by fitting a theoretical model to experimental data. However, with the exception of ref. 14–16, the best fit of the numerical model is generally judged by eye. The technique reported here involves fitting the numerical model to the experimental results using a global minimisation process based upon the downhill simplex method.[19–21] In the analysis, the independent fitting parameters allow the sample's thickness, refractive indices and dispersion relation, helicoidal pitch, and tilt angle to be determined. Independent measurements of some of these parameters then allow the validity and accuracy of the technique to be examined.

The 4 × 4 matrix method in SmC* subphases

4 × 4 Matrix calculations provide a general method of solving Maxwell's equations for different optical systems. The method of predicting the selective reflection spectrum from cholesteric liquid crystals was derived by Berreman[2,22] in the 1970s, when he utilised a rotating dielectric tensor as a function of depth within the liquid crystal. In this study, a similar method was followed to calculate the optical properties of the SmC* subphases through the evaluation of the appropriate dielectric tensor.[11] The dielectric tensor of the ferroelectric liquid crystal phase in the laboratory frame is given by

$$\varepsilon_{fe} = \begin{pmatrix} \Gamma + \Psi\cos 2\phi & \Psi\sin 2\phi & \Delta\cos\phi \\ \Psi\sin 2\phi & -\Psi\cos 2\phi & \Delta\sin\phi \\ \Delta\cos\phi & \Delta\sin\phi & \bar{\varepsilon} + \delta\cos 2\theta \end{pmatrix}$$

where the parameters Γ, Ψ, Δ, α, and δ are defined by $\Gamma = (\alpha +$

$\varepsilon_2)/2$, $\Psi = (\alpha - \varepsilon_2)/2$, $\Delta = \delta\sin2\theta$, $\alpha = -\delta\cos2\theta$, $= (\varepsilon_1 + \varepsilon_3)/2$ and $\delta = (\varepsilon_1 - \varepsilon_3)/2$, ϕ is the rotation angle as a function of thickness, and θ is the optical tilt angle. The parameters ε_1 to ε_3 are the dielectric constants in the molecular frame of reference. The pitch of the system is accounted for within the expression by describing the rotation angle as a function of the sample's thickness.

The dielectric tensor of the antiferroelectric phase, ε_{afe}, was calculated by averaging the ferroelectric tensor over the two-layer substructure, which therefore becomes

$$\varepsilon_{afe} = \begin{pmatrix} \Gamma + \Psi\cos2\phi & \Psi\sin2\phi & 0 \\ \Psi\sin2\phi & \Gamma - \Psi\cos2\phi & 0 \\ 0 & 0 & \bar{\varepsilon} + \delta\cos2\theta \end{pmatrix}$$

These tensors replaced the cholesteric dielectric tensor used in Berreman's 4 × 4 matrix formulation, allowing the reflected and transmitted components of an incident polarised wave from a SmC* and SmC*$_A$ liquid crystal to be calculated numerically. It is also well known that the dielectric constants are a function of wavelength. This dependence was included within the calculations by allowing the refractive index to vary with wavelength in accordance with the Sellmier equation.[23] The numerical models were used in conjunction with a downhill simplex algorithm[19–21] to quantitatively fit the reflection spectra deduced numerically to the experimental results and measure several of the physical parameters of the liquid crystals. The primary aim of this approach was to develop a fast and versatile technique to investigate the refractive indices, pitch and optical tilt angle in chiral smectic liquid crystals. Consequently, not all possible parameters were included in the theoretical model. Specifically, this model neglects complex refractive indices, dispersion in the optical axis and multiple domains. Including all possible parameters within a computer model can be counterproductive. Despite improving the fits slightly, the large increase in the number of dimensions in parameter space can greatly increase the degeneracy of the problem. The approximations made here are commonly used in considering the reflection spectra or otherwise measuring physical properties of chiral smectic liquid crystals. The downhill simplex algorithm was chosen due to the requirement for evaluation of a single numerical function only and not its derivatives. This is a constraint imposed by using a numerical solution to deduce the reflection spectra. The theory does have some analytic solutions, for special cases such as normal incidence, but for multiple calculations of normal and non-normal incidence of various liquid crystal phases, this theory does provide the best method. The downhill simplex algorithm is also significantly faster than many other techniques that do not require derivatives such as grid searches. However, multi-dimensional optical problems often present the problem of degeneracy within even a small range of the fitted parameters. It is only through comparison with independent measurements of the parameters that the validity of the fitted values can be examined.

One of the aims of this work was to compare the values of physical parameters deduced from the numerical fits to independent measurements. For refractive index measurements, it was therefore necessary to be able to relate the indices measured using a refractometer to values parallel and perpendicular to the director, $n_\parallel$ and $n_\perp$ (note that biaxiality has been neglected in this work). This is readily achieved, as shown below, by replacing the dielectric constants in the tensors above with $n_\parallel$ and $n_\perp$, allowing the refractive index tensors in the laboratory frame to be determined.

In the molecular frame of reference, if the refractive index tensor is given by

$$\begin{pmatrix} n_\parallel & 0 & 0 \\ 0 & n_\perp & 0 \\ 0 & 0 & n_\perp \end{pmatrix}$$

and, following the same conventions as Dreher *et al.*[4] and Müller and Stegemeyer,[24] the quantities measured with a refractometer equate to a combination of the diagonal elements of the refractive index tensor in the laboratory frame. The value of $n_{e\ SmC^*}$ is equivalent to a combination of $n_\perp$ and $n_\parallel$, taking into account the optical tilt angle of the system. The measured value of $n_{o\ SmC^*}$ is also a result of averaging $n_\perp$ and $n_\parallel$, in this case taking into account the helical structure. Therefore, as in the cholesteric case, $n_{o\ SmC^*}$ is taken as the mean of the first diagonal element at $\phi = 0$ and $\pi/2$. The two simultaneous equations are identical for both the SmC* and SmC*$_A$ phases:

$$n_{o\ SmC^*} = \sqrt{\frac{1}{2}\left((\Gamma' + \Psi')^2 + (\Gamma' - \Psi')^2\right)} = \sqrt{\Gamma'^2 + \Psi'^2}$$

and

$$n_{e\ SmC^*} = \bar{n} + \delta'\cos2\theta$$

where now $\Gamma' = (\alpha' + n_\perp)/2$, $\Psi' = (\alpha' - n_\perp)/2$, $\alpha' = \bar{n} - \delta'\cos2\theta$, $\delta'\cos2\theta$, $\bar{n} = (n_\parallel + n_\perp)/2$ and $\delta' = (n_\parallel - n_\perp)/2$. Measuring $n_{o\ SmC^*}$ and $n_{e\ SmC^*}$ allows these simultaneous equations to be solved, calculating the values of $n_\perp$ and $n_\parallel$.

Experimental

The structures and phase sequences of the three liquid crystals investigated in this study are shown in Fig. 1. The compounds were synthesised at the Universities of Hull and Kent State; compounds **1** and **3** having been previously studied using X-ray scattering.[18,25–27] The transition temperatures shown in Fig. 1 were determined by optical microscopy and electro-optical techniques.[18]

Free-standing films of the liquid crystals were produced by spreading material in the smectic A phase across the circular opening (2 mm diameter) of a commercially available hot stage.

Compound 1

I 116.6 SmA 109.4 SmC* 99.0 SmC*$_{FI1}$ 97.8 SmC*$_A$

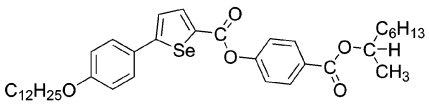

Compound 2

I 119.0 SmA 112.6 SmC* 86.3 SmC*$_{FI1}$ 81.8 SmC*$_{FI2}$ 79.6 SmC*$_A$

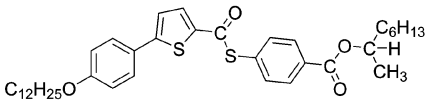

Compound 3

I 96.8 SmA 87.6 SmC*$_a$ 85.8 SmC* 82.8 SmC*$_{FI1}$ 80.3 SmC*$_A$

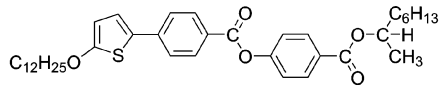

Fig. 1 The structures and phase sequences of the three materials studied. All transition temperatures are in °C and were determined by microscopy and electro-optical measurements. SmC*$_{FI1}$ and SmC*$_{FI2}$ denote the three- and four-layer intermediate phases, respectively.[17]

The hot stage was fully enclosed and thermally insulated to provide a temperature stability of ±0.1 °C. The sample geometry obtained using the free-standing film was quasi-homeotropic, with the helicoidal axis in the chiral phases parallel to both the microscope axis and the smectic layer normals. In addition to providing excellent mono-domain alignment, the use of free-standing films simplifies the theoretical analysis of the reflection spectra, as the film is bounded on each side by air. This is in contrast to selective reflection from devices where multiple refractive index boundaries from air, substrate, electrode and alignment layers need to be considered.

The apparatus used to measure the selective reflection spectra of the chiral smectic phases operates only at visible wavelengths. Consequently, prior to recording the spectra, observations were made to determine in which phase each material exhibited selective reflection at visible wavelengths. Each of the compounds reflected visible light in either the SmC* phase (compounds **1** and **2**) or the SmC*$_A$ phase (compound **3**). As expected, no selective reflection was observed in the intermediate (ferrielectric) phases. Reflection spectra were obtained using a modified reflecting and polarising microscope coupled to a monochromator. White light was incident on the sample *via* a 10× objective with a numerical aperture of 0.2. This was selected specifically because of the small cone angle of light incident on the sample, allowing the geometry to be considered as normal illumination. In order to justify this assumption, the spectra for normal incidence as well as the maximum angles of incidence and reflection were calculated. The theoretical data obtained were compared with experimental data using different incident cone angles. For the objective lens and numerical aperture chosen for this experiment, the theoretical fits indicated that the optical geometry can be considered as normal incidence to a very good approximation. Light reflected from the sample was passed into a LabVIEW™-controlled Chromex 500IS imaging spectrometer, dispersed, and detected by a Hamamatsu R636-10 photomultiplier tube. The resolution of the monochromator was determined by the grating used (1200 lines cm^{-1}) and by the width of the entrance and exit slits. Previous calibrations[28] with standard wavelength sources showed the spectrometer to be accurate to ±0.05 nm with the slit width used in this experiment. The reflection spectra obtained using this apparatus were normalised to take into account the chromatic response of the system.

Measurements of the refractive indices were made using an Abbé refractometer and a sodium lamp light source (wavelength 589.6 nm). Temperature control was provided by a thermostatic water bath with an accuracy ±0.2 °C and a maximum achievable temperature of 80 °C, so all measurements were made in the antiferroelectric phases only. Reasonable homeotropic alignment of the samples was achieved using a lecithin alignment layer, though it should be noted that the quality of alignment and, hence, the accuracy of the measurements, was not as good as would be expected for nematic samples. The data obtained from the refractometer were analysed as a function of temperature using the supplied standard prism index data, independently measured optical tilt angle[26,29] and the mathematical theory described in the previous section.

Results and discussion

Fig. 2 shows typical reflection spectra determined experimentally for each of the three compounds, together with corresponding numerical fits to the data. In this and all subsequent figures, the reduced temperature is defined as the temperature below the SmC* to SmA phase transition, $T - T_{C^*-A}$. The goodness-of-fit was measured in all cases using the

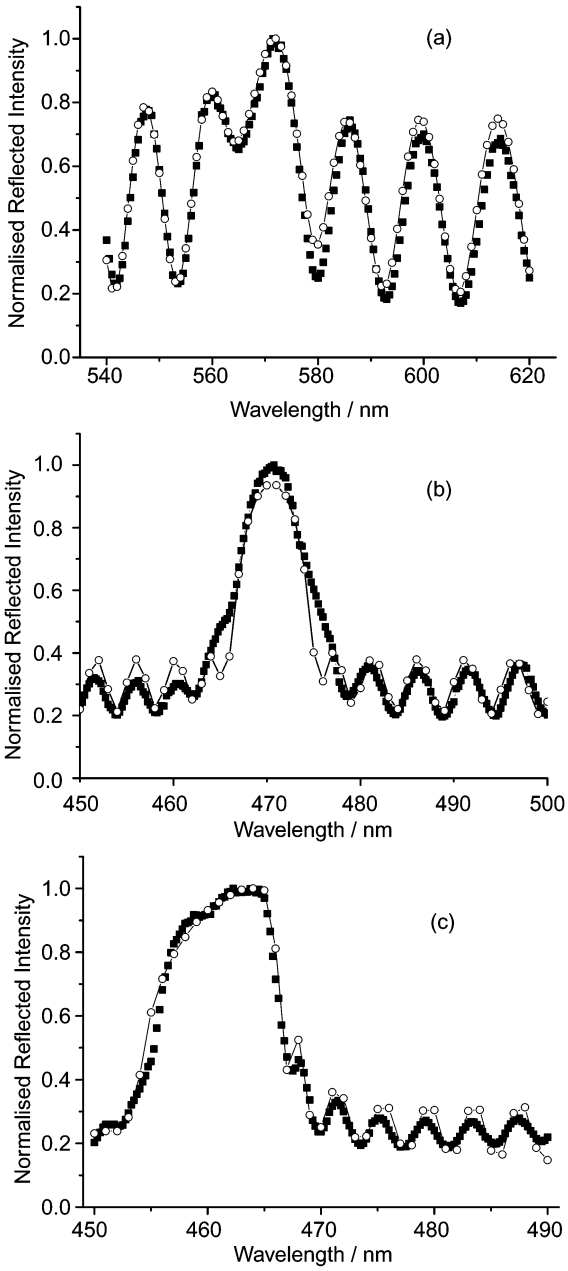

Fig. 2 Experimental reflection spectra (■) and corresponding numerical fits (○) for (a) compound **1** (−8.0 °C), (b) compound **2** (−1.0 °C) and (c) compound **3** (−10.5 °C). Quoted temperatures are reduced temperatures, $T - T_{C^*-A}$, where T_{C^*-A} is the SmC* to SmA transition temperature.

standard χ^2 test, and these statistical data are included in Table 1. The goodness-of-fit proves that, at a 5% significance level, the model can be used to predict the correct experimental features for all materials. The fitting procedure typically takes around 20 min per spectrum with a Pentium 4 1.7 GHz desktop personal computer. The plots clearly show two features: the selective reflection peak and multiple thin film interference peaks. The shape of the reflection peak differs in each of the plots and this aspect of the spectra will be discussed later. In each of the graphs, the width of the reflection peaks is of the order of 20 nm, which is somewhat smaller than the typical peak width from selective reflection in cholesteric systems. The reduction in peak width is a result of the reduction in the effective birefringence of the sample, in turn a consequence of the director tilt. It should be noted that better fits *can* be made to the selective reflection peaks alone, but at the cost of far worse fits over the remainder of the spectrum. Such effects have

Table 1 Statistical data relating to the goodness-of-fit for compounds **1**–**3** in Fig. 2

	Compound **1** [Fig. 2(a)]	Compound **2** [Fig. 2(b)]	Compound **3** [Fig. 2(c)]
Chi-squared value	59.9	130.2	65.3
Number of degrees of freedom	161	201	161
Level of significance	>0.05	>0.05	>0.05

been observed by others.[30] It is considered here that for our relatively simple model, a good fit over a wide wavelength range is more relevant than a restricted wavelength fit. Of course, including such properties as weak absorption should improve the fits further over the whole wavelength range, something that will be considered in future developments.

The fits to the reflection data produce the refractive indices (as a function of wavelength), helicoidal pitch, optical tilt angle and sample thickness. To investigate the accuracy of the fitting method, several independent measurements of refractive indices and pitch were compared to the calculated values. Fig. 3(a) and (b) show the comparison between the refractive indices $n_{\perp}$ and $n_{\parallel}$ measured using the Abbé refractometer and those deduced from the reflection spectra. All values are quoted at a wavelength of 589.6 nm. In this and all subsequent figures, only a single typical error bar has been plotted for each data set for graphical clarity. Fig. 3(a) and (b) both show good agreement between data sets; the measurements made using the refractometer and those deduced numerically lying within two standard deviations of one another. Fig. 3(c) shows the refractive indices in the SmC^*_A phase for compound **3** deduced from fitting alone. This was a result of insufficient quantities of compound **3** being available for the refractometer measurements. The good agreement between the measured and calculated data sets shows that the fitting technique is a reliable method for determining the refractive indices of SmC* systems (in uniaxial approximation), though it does not appear to be quite as accurate as the direct measurement. Nonetheless, deducing the refractive indices from reflection spectra has several advantages over measurements made using a refractometer. Firstly, the fits allow the rapid measurement of the dispersion relation of a material as a function of temperature. Furthermore, far less sample is needed for the measurement of reflection spectra than is required to adequately fill the sample space on a refractometer, an important consideration for many materials, including those studied here. Finally, the temperature range of the hot stage is much broader than that of standard refractometers, which rarely operate at temperatures exceeding 100 °C.

Fig. 4 shows the optical tilt angles of the three compounds deduced from the fits and compared with independent measurements made using electro-optical switching techniques. Again, the two data sets show good overall agreement, though Fig. 4(a) and (b) have a relatively large mismatch in the pre-transitional region. There are several possible reasons for the differences in the data sets. Firstly, the experimental geometries were different. The electro-optical measurements are made under the influence of an electric field in a planar device, while the reflection spectra are obtained with no applied field and in a homeotropic free-standing film geometry. It has been shown elsewhere that surface alignment strongly influences optical measurements of the tilt angle[14] and also that confined or restricted geometries (such as occurs with a highly chiral smectic sample in a planar device) can have a significant influence on the physical properties of such phases.[31–33] There are two other reasons that the data could differ. The first is that dispersion in the optical axis has been neglected in our model. However, in making the tilt angle constant with wavelength in the calculations, we are mirroring the use of white light in the electro-optical measurements, both of which effectively give an average value for tilt. Therefore, it seems unlikely that

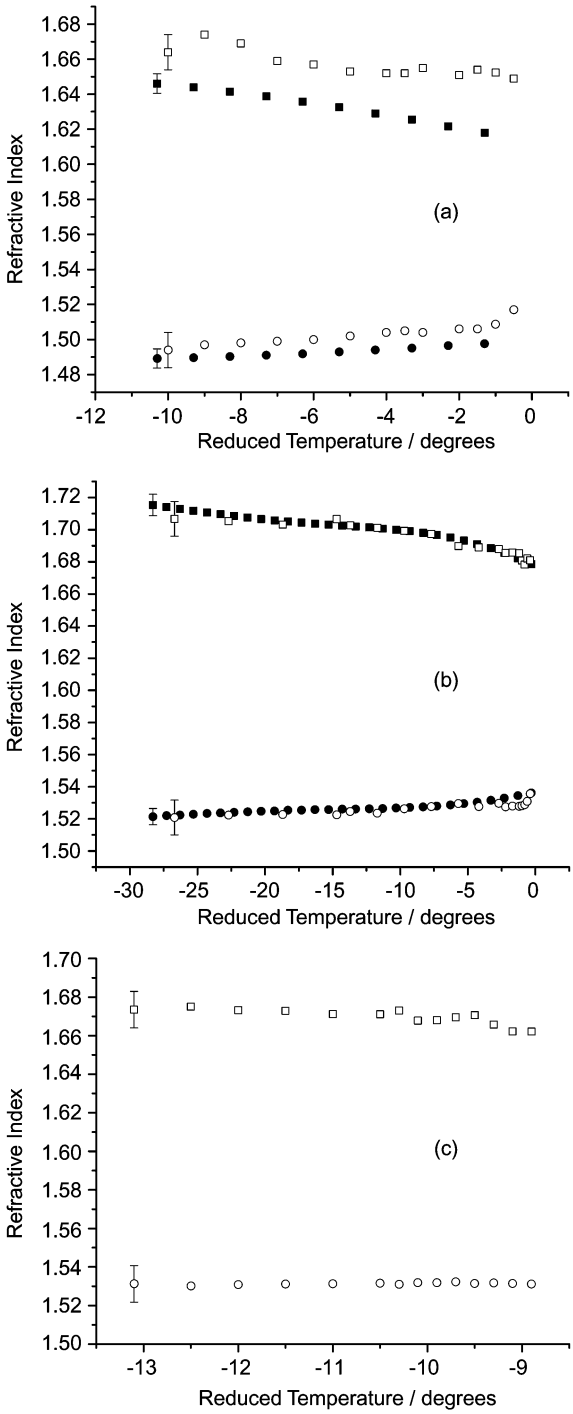

Fig. 3 Comparison between measured refractive indices, $n_{\parallel}$ (■) and $n_{\perp}$ (●), and the corresponding reflection spectra fitting, $n_{\parallel}$ (□) and $n_{\perp}$ (○), for (a) compound **1**, (b) compound **2** and (c) compound **3**. Results for compounds **1** and **2** were measured in the SmC* phase and compound **3** was measured in the SmC^*_A phase. Reduced temperatures are $T - T_{C^*-A}$, where T_{C^*-A} is the SmC* to SmA transition temperature. Uncertainties associated with the calculated data were deduced using standard numerical methods.

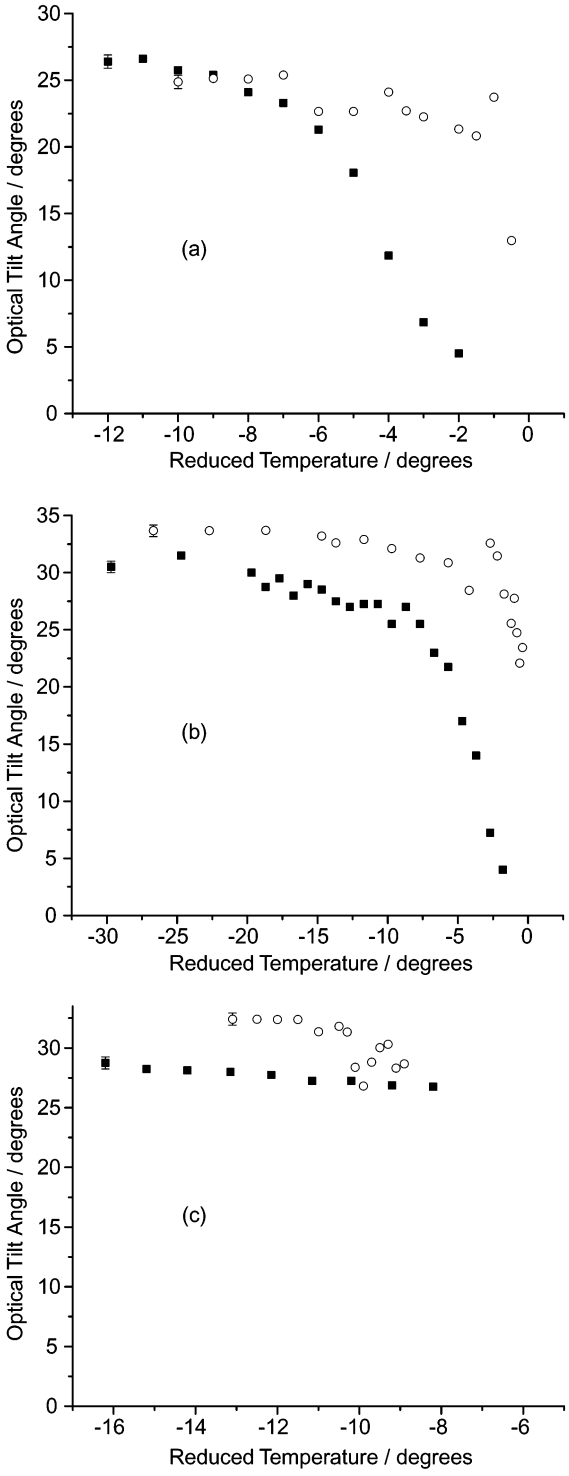

Fig. 4 Temperature evolution of the electro-optically measured optical tilt angle (■) and the corresponding reflection spectra fitting (○) for (a) compound **1**, (b) compound **2** and (c) compound **3**. Results for compounds **1** and **2** were measured in the SmC* phase and compound **3** was measured in the SmC*$_A$ phase. Reduced temperatures are $T - T_{C^*-A}$, where T_{C^*-A} is the SmC* to SmA transition temperature.

this omission from the model is causing the discrepancy. The derived data differs most markedly from the electro-optical data in the pre-transitional region, where the tilt becomes small. It is important to consider whether the difference could therefore be attributed to limiting the model to normal angles of incidence only. Calculations of the peak profile under varying angles of incidence at low optical tilt angles (5–10°) conclusively show that this is not the case; the experimental data obtained in the pre-transitional region can only be fit to an optical tilt angle of the order of 20° or greater. Therefore, we conclude that the most likely explanation for the differences between data sets in Fig. 4(a) and (b) is the differences in measurement geometry and application of external influences, such as the electric field.

One of the principal benefits of applying the fitting procedure to the selective reflection spectra is that it is possible to determine the helical pitch of the material, rather than the just position of the centre of the reflection peak, as has been reported elsewhere.[7–10] Since the shape of the reflection peak can vary depending on the experimental conditions, fitting to the data gives a more reliable and useful measure of the pitch of the chiral smectic phases. For example, in thicker free-standing films (>10 μm), the sides of the reflection spectrum profile slope, making it difficult to determine the positions of the sides and centre of the peak reliably. The slope is due to the coupling of the effective birefringence, sample thickness and incident polarisation. The former effect is illustrated in Fig. 2(b) and (c), where the sloping sides of the reflection band make it difficult to ascribe a position to the sides of the peak. Fig. 5 shows the calculated change in the position of the centre of the peak as a function of the angle of incident polarisation with respect to the surface director of the liquid crystal. This change in the profile of the reflection spectrum is analogous to that seen in cholesterics,[34] but again, without knowing the incident polarisation/surface director relationship, it introduces an error into the measurment of the centre of the reflection peak.

Fig. 6 shows the helical pitch of compounds **1**–**3** as a function of temperature. The measurements in the SmC* phase of compounds **1** and **2** show a divergence of the pitch in the pre-transitional regime, where the pitch reduces as the SmA phase is approached, as has been observed for other SmC* materials.[7] In contrast, the pitch data in the SmC*$_A$ phase in compound **3** show only a decrease as a function of increasing temperature. The rapid increase in pitch at the transition to intermediate phases was observed by eye as a shift in the selective reflection to longer wavelengths, but the temperature stability of the hot stage did not allow this rapid change to be detected by the monochromator apparatus.

Resonant X-ray scattering data[27] for compound **1** provide a comparison of the calculated pitch values presented here to those deduced independently. At a reduced temperature of −5.3 °C, Matkin *et al.*[27] measured the pitch of compound **1** to be 390 ± 10 nm. This compares well to the pitch calculated by the numerical fit to the reflection spectra of 364 ± 2 nm. A similar level of agreement is found between the results presented here and pitch measurements made from other

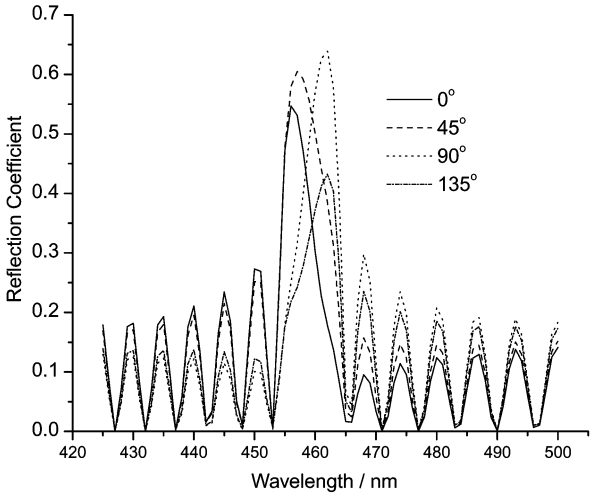

Fig. 5 Change in profile of the reflection spectra as a function of the angle between the incident linear polarisation and the surface director. Note the translation of the peak maximum.

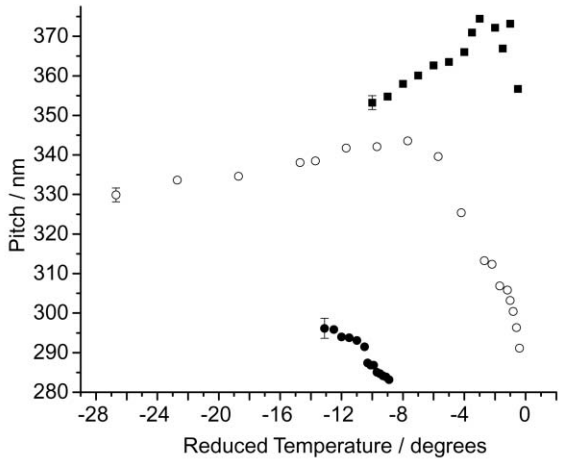

Fig. 6 Evolution of the helical pitch as a function of temperature for compound **1** (■), compound **2** (○) and compound **3** (●). Results for compounds **1** and **2** were measured in the SmC* phase and compound **3** was measured in the SmC^*_A phase. Reduced temperatures are $T - T_{C^*-A}$, where T_{C^*-A} is the SmC* to SmA transition temperature.

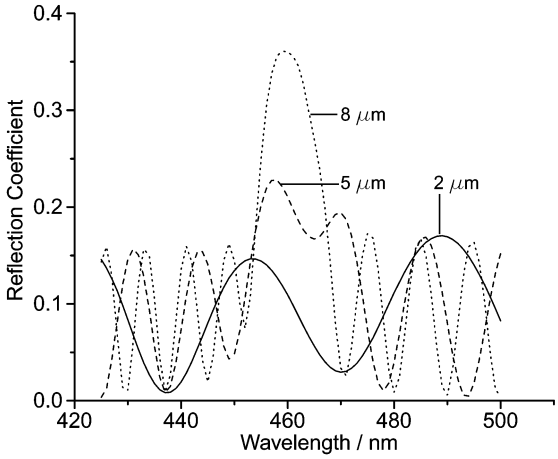

Fig. 7 Calculated reflection spectra of a SmC* phase as a function of film thickness. Parameters used in the calculation: $n_{\|}$ 1.65; $n_{\perp}$ 1.52; pitch 300 nm; optical tilt angle 25°; incident polarisation perpendicular to the surface alignment.

resonant X-ray experiments.[25,27] The comparatively short pitch in the antiferroelectric phase of compound **3** is as expected given the even shorter pitch previously measured in the SmC* and SmC_α phases.[18]

In the case of thin free-standing films, the profile of the reflection peak totally prevents any simple peak analysis to provide a calculation of the pitch, as in Fig. 2(a). Assigning any position on the spectrum as upper, middle or lower positions of the peak, which could in principle correspond to simple combinations of the pitch and ordinary, extraordinary or average refractive indices, would be purely arbitrary. Therefore the fitting method employed here provides a considerably more accurate alternative to measuring the pitch in such thin film smectic systems.

The double peaked profile of the reflection spectrum shown in Fig. 2(a) is typical of many thin sample reflection spectra. Bahr and Fliegner[35] attributed this profile in thin free-standing films to a π-wall domain structure seen in their experiments. While we can not rule out a contribution to the profile of the reflection band from such a director field, the free-standing films used in our experiments were mono-domain films. Furthermore, when the thickness of the film and the refractive indices cause the thin film interference fringes to be approximately half the spacing of the width of the reflection band, a double peak structure in the profile can be clearly seen. If the film is thicker, then the profiles of the peaks appear more akin to a cholesteric reflection band, as in Fig. 2(b) and (c), spread over many interference fringes. If the film is much thinner, the reflection band is not visible and only a few interference fringes are seen across the visible spectrum. This phenomenon is also observed in cholesteric reflection spectra, where the sample needs to be 5–10 pitches thick before the reflection band takes on its typical profile.[6] Fig. 7 shows the numerically calculated spectra of three examples of different thicknesses. Solving Maxwell's equations for both the ferroelectric and antiferroelectric architectures predicts the described effect and, clearly, the profiles of the reflection spectra are greatly influenced by the thickness of the film in a single mono-domain sample due to the effective birefringence. We therefore attribute the double peaked structure to a coupling between the thin film interference fringes and the reflection band.

Conclusion

This study demonstrates that the numerical fitting of experimental reflection spectra from chiral liquid crystal systems allows many of the important physical parameters of these systems to be calculated with good levels of accuracy. Independent measurements of the refractive indices of compounds **1** and **2** confirm the validity of the fitting procedure. The speed of the fitting process and the ability to measure the dispersion relation as a function of temperature make this an extremely efficient technique. The temperature dependence of the optical tilt and pitch for compounds **1**–**3** was also analysed, showing the expected general trends, especially in the pitch divergence at the SmC* to SmA transition.

Furthermore, in free-standing films of thickness in the range 5–10 μm, double peak reflection spectra from mono-domain samples were measured. Numerical calculations show these to be attributable to the existence of the thin film interference peaks, proving the profile of the reflection peak to be an important function of the sample thickness and incident polarisation.

Acknowledgement

We thank the EPSRC for financial support.

References

1 H. L. De Vries, *Acta Crystallogr.*, 1951, **4**, 219.
2 D. Berreman, *J. Opt. Soc. Am.*, 1972, **62**(4), 502–510.
3 C. Oldano, *Phys. Rev. A*, 1989, **40**(10), 6014–6020.
4 R. Dreher, G. Meier and A. Saupe, *Mol. Cryst. Liq. Cryst.*, 1971, **13**(1), 17–26.
5 H. F. Gleeson and H. J. Coles, *Mol. Cryst. Liq. Cryst.*, 1989, **170**, 9–34.
6 W. D. St. John, W. J. Fritz, Z. J. Lu and D. K. Yang, *Phys. Rev. E*, 1995, **51**(2), 1191–1198.
7 J. Li, H. Takezoe and A. Fukuda, *Jpn. J. Appl. Phys.*, 1991, **30**(3), 532–536.
8 T. Akizuki, K. Miyachi, Y. Takanishi, K. Ishikawa, H. Takezoe and A. Fukuda, *Jpn. J. Appl. Phys.*, 1999, **38**(8), 4832–4837.
9 J. Phillip, J. R. Lalanne, J. P. Marcerou and G. Sigaud, *Phys. Rev. E*, 1995, **52**(2), 1846–1856.
10 M. Kawaida, M. Nakagawa and T. Akahane, *Jpn. J. Appl. Phys., Part 2*, 1988, **27**(8), L1365–L1367.
11 I. Muševic, R. Blinc and B. Zekš, *The Physics of Ferroelectric and Antiferroelectric Liquid Crystals*, World Scientific, Singapore, 2000, p. 200.
12 P. M. Johnson, D. A. Olson, S. Pankratz, H. T. Nguyen, J. W. Goodby, M. Hird and C. C. Huang, *Phys. Rev. Lett.*, 2000, **84**(21), 4870–4873.
13 N. M. Shtykov, J. K. Vij and H. T. Nguyen, *Phys. Rev. E*, 2001, **63**(5-1), 51 708/1–51 708/7.
14 F. Y. Yang, G. W. Bradberry and J. R. Sambles, *Phys. Rev. E*, 1994, **50**(4), 2834–2838.

15 F. Y. Yang, G. W. Bradberry and J. R. Sambles, *Phys. Rev. E*, 1996, **53**(1-A), 674–680.
16 F. Yang, J. R. Sambles and G. W. Bradberry, *J. Appl. Phys.*, 1995, **78**(4), 2187–2192.
17 A. Cady, J. A. Pitney, R. Pindak, L. S. Matkin, S. J. Watson, H. F. Gleeson, P. Cluzeau, P. Barois, A.-M. Levelut, W. Caliebe, J. W. Goodby, M. Hird and C. C. Huang, *Phys. Rev. E*, 2001, **64**(5-1), 50 702/1–50 702/4.
18 L. S. Hirst, S. J. Watson, P. Cluzeau, P. Barois, R. Pindak, J. Pitney, A. Cady, P. M. Johnson, C. C. Huang, A.-M. Levelut, G. Srajer, J. Pollmann, W. Caliebe, A. Seed, M. R. Herbert, J. W. Goodby and M. Hird, *Phys. Rev. E*, 2002, **65**(4-1), 41 705/1–41 705/10.
19 J. A. Nelder and R. Mead, *Comput. J.*, 1965, **7**, 308–313.
20 J. M. Parkinson and D. Hutchinson, in *Numerical Methods for Nonlinear Optimization*, ed. F. A. Lootsma, Academic Press, New York, 1972, p. 115–135.
21 W. H. Press, B. P. Flannery, S. A. Teukolsky and W. T. Vetterking, *Numerical Recipes in C*, Cambridge University Press, Cambridge, 1988, p. 305.
22 R. M. A. Azzum and N. M. Bashara, *Ellipsometery and Polarized Light*, Elsevier Science B.V., Amsterdam, 1996, p. 340.
23 F. A. Jenkins and H. E. White, *Fundamentals of Optics*, 4th Edition, McGraw-Hill International Editions, Aukland, 1981, p. 482.
24 W. U. Müller and H. Stegemeyer, *Ber. Bunsen-Ges. Phys. Chem.*, 1973, **77**(1), 20–23.
25 L. S. Matkin, S. J. Watson, H. F. Gleeson, R. Pindak, J. Pitney, P. M. Johnson, C. C. Huang, P. Barois, A.-M. Levelut, G. Srajer, J. Pollmann, J. W. Goodby and M. Hird, *Phys. Rev. E.*, 2001, **64**(2-1), 211 705/1–211 705/6.
26 S. J. Watson, L. S. Matkin, L. J. Baylis, N. Bowring, H. F. Gleeson, M. Hird and J. Goodby, *Phys. Rev. E*, 2002, **65**(3-1), 31 705/1–31 705/9.
27 L. S. Matkin, H. F. Gleeson, P. Mach, C. C. Huang, R. Pindak, G. Srajer, J. Pollmann, J. W. Goodby, M. Hird and A. Seed, *Appl. Phys. Lett.*, 2000, **76**(14), 1863–1865.
28 J.-P. Guillou, MSc Thesis, University of Manchester, UK, 2000, p. 35.
29 J. Conn, Personal Communication.
30 V. A. Belyakhov and V. E. Dmitrienko, *Optics of Chiral Liquid Crystals*, Soviet Scientific Reviews/Section A, Physics Reviews 13(1), Harwood Academic Publishers, New York, 1989.
31 J. P. F. Lagerwall, D. D. Parghi, D. Krüerke, F. Gouda and P. Jägemalm, *Liq. Cryst.*, 2002, **29**(2), 163–178.
32 W. K. Robinson, Ph.D. Thesis, University of Manchester, UK, 1995, p. 138.
33 K. Itoh, M. Kabe, K. Miyanchi, Y. Takanishi, K. Ishikawa, H. Takezoe and A. Fukuda, *J. Mater. Chem.*, 1997, **7**(3), 407–416.
34 M. Tur, *Mol. Cryst. Liq. Cryst.*, 1975, **29**, 345–359.
35 C. H. Bahr and D. Fliegner, *Liq. Cryst.*, 1993, **14**(2), 573–580.